The Astrophysical Journal, 761:4 (13pp), 2012 December 10 doi:10.1088/0004-637X/761/1/4
© 2012. The American Astronomical Society. All rights reserved. Printed in the U.S.A.

INVESTIGATING THE OPTICAL COUNTERPART CANDIDATES OF FOUR *INTEGRAL* SOURCES LOCALIZED WITH *CHANDRA*

Mehtap Özbey Arabacı[1], Emrah Kalemci[2], John A. Tomsick[3], Jules Halpern[4], Arash Bodaghee[3], Sylvain Chaty[5,6], Jerome Rodriguez[5], and Farid Rahoui[7,8]
[1] Department of Physics, Middle East Technical University, Ankara, 06531, Turkey; mehtap@astroa.physics.metu.edu.tr
[2] Faculty of Engineering and Natural Sciences, Sabancı University, Orhanlı-Tuzla, İstanbul, 34596, Turkey
[3] Space Sciences Laboratory, 7 Gauss Way, University of California, Berkeley, CA 94720-7450, USA
[4] Columbia Astrophysics Laboratory, Columbia University, 550 West 120th Street, New York, NY 10027-6601, USA
[5] AIM (UMR-E 9005 CEA/DSM-CNRS-Université Paris Diderot) Irfu/Service d'Astrophysique, Centre de Saclay, F-91191 Gif-sur-Yvette Cedex, France
[6] Institut Universitaire de France, 103, Bd Saint-Michel, F-75005 Paris, France
[7] Astronomy Department, Harvard University, 60 Garden Street, Cambridge, MA 02138, USA
[8] Harvard-Smithsonian Center for Astrophysics, 60 Garden Street, Cambridge, MA 02138, USA
Received 2012 August 17; accepted 2012 October 15; published 2012 November 19

ABSTRACT

We report on the optical spectroscopic follow-up observations of the candidate counterparts to four *INTEGRAL* sources: IGR J04069+5042, IGR J06552−1146, IGR J21188+4901, and IGR J22014+6034. The candidate counterparts were determined with *Chandra*, and the optical observations were performed with 1.5 m RTT-150 telescope (TÜBİTAK National Observatory, Antalya, Turkey) and 2.4 m Hiltner Telescope (MDM Observatory, Kitt Peak, Arizona). Our spectroscopic results show that one of the two candidates of IGR J04069+5042 and the one observed for IGR J06552−1146 could be active late-type stars in RS CVn systems. However, according to the likelihood analysis based on *Chandra* and *INTEGRAL*, two optically weaker sources in the *INTEGRAL* error circle of IGR J06552−1146 have higher probabilities to be the actual counterpart. The candidate counterparts of IGR J21188+4901 are classified as an active M-type star and a late-type star. Among the optical spectra of four candidates of IGR J22014+6034, two show Hα emission lines, one is a late-type star, and the other is an M type. The likelihood analysis favors a candidate with no distinguishing features in the optical spectrum. Two of the candidates classified as M-type dwarfs, are similar to some IGR candidates claimed to be symbiotic stars. However, some of the prominent features of symbiotic systems are missing in our spectra, and their NIR colors are not consistent with those expected for giants. We consider the IR colors of all IGR candidates claimed to be symbiotic systems and find that low-resolution optical spectrum may not be enough for conclusive identification.

Key words: stars: activity – stars: flare – stars: individual (IGR J04069+5042, IGR J06552−1146, IGR J21188+4901, IGR J22014+6034) – stars: late-type – X-rays: stars

Online-only material: color figures

1. INTRODUCTION

The *International Gamma-Ray Astrophysics Laboratory* (*INTEGRAL*; Winkler et al. 2003) has discovered hundreds of new hard X-ray sources (so-called IGR sources) at energies above 20 keV since its launch in 2002 October. Out of over 700 sources that are listed in the 4th Bird Catalog (Bird et al. 2010), more than 400 are exclusively IGR sources.[9] *INTEGRAL* is very successful in finding new hard X-ray sources thanks to its wide field of view (FOV), observing strategy, and, most importantly, the unique imaging capability of the ISGRI detector (Lebrun et al. 2003) with a localization accuracy of a few arcminutes. However, such localization accuracy is often not enough to identify the correct optical counterparts of these sources. Without multiwavelength information, it may not be possible to understand the physical origin of the X-ray emission and type of the emitting system. To identify a unique optical or infrared counterpart, arcsecond accuracy localization of the X-ray source is required.

Our group observes the positions of IGR sources with soft X-ray telescopes such as *Chandra* and *Swift*, not only for identifying the correct counterparts, but also for producing 0.3–10 keV spectra that can be used to measure column densities and continuum shapes (Tomsick et al. 2006, 2009, 2012; Rodriguez et al. 2008, 2009, 2010).

From such spectroscopic and imaging efforts, it was possible to identify the nature of a large fraction of these IGR sources (Chaty et al. 2008; Butler et al. 2009; Masetti et al. 2007, 2008, 2012 and references therein). Among these sources >250 are active galactic nuclei. The Galactic sources include high-mass X-ray binaries, low-mass X-ray binaries and cataclysmic variables, isolated neutron star (NS) systems as well as supernova remnants and pulsar wind nebulae. Yet, the nature of one-third of IGR sources has not been identified. The identifications include a low number of unexpected hard X-ray sources like RS Canes Venatici (RS CVn), and symbiotic binary systems (Bird et al. 2010; Masetti et al. 2012; Rodriguez et al. 2010), and thus searches for more such objects are warranted.

So far, there have been four IGR sources tentatively identified as RS CVn binaries (Rodriguez et al. 2010; Masetti et al. 2012; Krivonos et al. 2010), but no firm association with RS CVn systems and IGR sources exists. In general, RS CVn systems are the members of chromospherically active stars which include flare stars (dMe stars or UV Ceti stars) and T Tauri stars as well. These systems are detached binaries having emission lines of Ca II H & K and Hα lines in their optical spectra.

The components of an RS CVn system can be G–M-type stars within the luminosity classes of II–V (Kogure & Leung 2007).

[9] See http://irfu.cea.fr/Sap/IGR-Sources/ for an updated list.

Table 1
The X-Ray Measurements of IGR Sources Given in Bird et al. (2010)

IGR Name	R.A.(J2000)	Decl.(J2000)	l[a]	b[b]	Error Radius[c]	$\text{Flux}_{20-40\ \text{keV}}$	$\text{Flux}_{40-100\ \text{keV}}$	Peak Flux[d] $_{20-40\ \text{keV}}$
J04069+5042	$04^h06^m55^s.0$	$+50°42'.1$	151.43	−1.03	4′.2	1.6 ± 0.3	<1.0	2.0 ± 0.3
J06552−1146	$06^h55^m10^s.0$	$-11°46'.2$	223.85	−4.52	4′.3	1.1 ± 0.3	<1.0	2.6 ± 1.0
J21188+4901	$21^h18^m48^s.0$	$+49°01'.0$	91.27	−0.33	4′.3	<0.2	<0.4	4.5 ± 1.3
J22014+6034	$22^h01^m27^s.0$	$+60°34'.0$	103.49	+4.28	5′.4	<0.2[e]	<0.4	...

Notes. The fluxes are given in units of mCrab. A flux of 1 mCrab in the 20–40 keV energy range corresponds to 7.57×10^{-12} erg cm^{-2} s^{-1} while it is 9.42×10^{-12} erg cm^{-2} s^{-1} for 40–100 keV band.
[a] The Galactic longitude of the source in degrees.
[b] The Galactic latitude of the source in degrees.
[c] The radius of the 90% confidence IGR circle.
[d] The peak flux of the sources which show variability in the 20–40 keV energy band. For IGR J22014+6034 no variation detected in this range.
[e] The source is detected in 17–30 keV band, Bird et al. (2010).

This type of system is known to have strong X-ray and radio emission (Barbier et al. 2005; Osten et al. 2007). They show solar-like magnetic activities and flares (Haisch et al. 1990).

Symbiotic systems are long-period interacting binaries consisting of a red giant star (G–M) and a hot companion surrounded by an ionized nebula (Friedjung & Viotti 1982; Kenyon 1986, 1990; Kenyon & Webbink 1984). The hot component is most often a white dwarf or a disk-accreting main-sequence star. On the other hand, there are also systems having an NS as the compact companion (Mikołajewska et al. 1997). In general, the optical spectra of symbiotic stars have photospheric absorption features and molecular bands of the cool giant and emission lines of the H I Balmer series, He I, He II, [O III], and [Ne III] which are produced in the surrounding nebula of the hot component by its intense UV radiation (Kenyon & Fernandez-Castro 1987; Cieslinski et al. 1994). In addition, these systems can show hard, soft, and supersoft X-ray emissions (Kennea et al. 2009; Muerset et al. 1997).

So far, 11 IGR sources have been suggested to be symbiotic systems according to their optical/infrared features and X-ray properties. Among those identified, the symbiotic nature of IGR J10109−5746 (CD−57 3057; Masetti et al. 2006; Kennea et al. 2009), IGR J12349−6434 (RT Cru; Masetti et al. 2005; Luna & Sokoloski 2007; Kennea et al. 2009), and IGR J16194−2810 (Masetti et al. 2007; Ratti et al. 2010) are well determined through multiwavelength analyses. A nearby system (1.56 kpc, parallax measurement), IGR J15293−5609, has been classified as a symbiotic binary based on the well-determined surface temperature and radius of the companion star (Tomsick et al. 2012). On the other hand, the identifications of IGR J16358−4726 (Nespoli et al. 2010) and IGR J17497−2821 (Paizis et al. 2007, 2009) as symbiotic systems are questionable. Chaty et al. (2008) suggest that IGR J16358−4726 could be a high-mass X-ray binary. Likewise, the classification of IGR J17497−2821 is also controversial due to the suggestion of a black hole primary (Walter et al. 2007; Paizis et al. 2007) would make the system very unusual among the known symbiotics. IGR J16393−4643 was also claimed to be a symbiotic system based on the *K*-band spectrum of the candidate counterpart 2MASS J16390535−4642137 (Nespoli et al. 2010) which was previously classified as a BIV–V-type star using its optical/IR spectral energy distribution (Chaty et al. 2008). Later, it was revealed that the refined X-ray position of IGR J16393−4643 was incompatible with this controversial Two Micron All Sky Survey (2MASS) source (Bodaghee et al. 2012).

Candidate counterparts to IGR J11098−6457, IGR J17197−3010, and 1RXS J174607.8−213333 (Masetti et al. 2009, 2012, 2008) are also tentatively claimed to be late M-type giants based on comparison of their optical spectra with the known symbiotic systems, but it was later shown that the tentative optical counterpart identifications of IGR J11098−6457 and IGR J17197−3010 are wrong (Tomsick et al. 2009; Luna et al. 2012). Finally, IGR J16293−4603 was suggested to be a candidate symbiotic system by Ratti et al. (2010) based solely on its optical/NIR photometry.

In this work, we investigated the optical candidate counterparts of four IGR sources in the 4th Bird Catalog (Bird et al. 2010) with unknown X-ray classification: IGR J04069+5042, IGR J06552−1146, IGR J21188+4901, and IGR J22014+6034. The fields of these sources were observed with *Chandra*, and possible optical/infrared counterparts were identified (Tomsick et al. 2012, hereafter T12). All four sources have low Galactic latitudes (see Table 1), and high extinction limits the possible counterparts mostly to relatively nearby stellar objects. We performed optical spectroscopy of bright candidates in the United States Naval Observatory (USNO) and 2MASS catalogs, and also obtained images that were located near the brightest *Chandra* sources. This work is follow up of T12 that utilized *Chandra* to find X-ray counterparts of IGR sources for further investigations.

The paper is organized as follows. In Section 2, we summarize the observations and data reduction in the optical, in Section 3 we identify the types of optical counterpart candidates of the IGR sources, and in the final section, we discuss the possible counterparts to each IGR source, and compare the M-type candidates we found with earlier tentative symbiotic identifications.

2. OBSERVATIONS AND DATA REDUCTION

The *INTEGRAL* coordinates and the fluxes of the four sources we investigated are given in Table 1. The *Chandra* localizations (see Table 2) of the candidate counterparts allowed us to select sources to be observed at the TÜBİTAK Turkish National Observatory[10] (TUG) and at the MDM Observatory. A detailed list of all detected possible *Chandra* counterparts and their soft X-ray properties are reported in T12. All of the X-ray sources detected by *Chandra* in the field of each IGR source are shown in Figure 1. We also searched the online catalogs of 2MASS, USNO-B1.0, and USNO-A2.0 to find the IR and optical counterparts associated with the *Chandra* positions (see Table 3).

[10] http://www.tug.tubitak.gov.tr

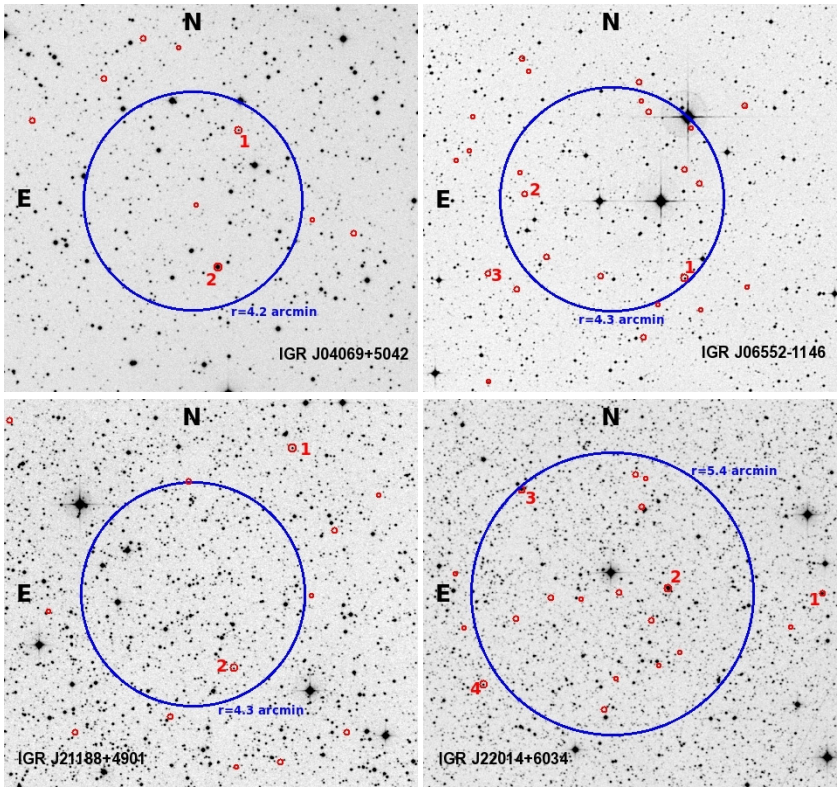

Figure 1. DSS-R images of the fields around IGR J04069+5042 (upper left panel), IGR J06552−1146 (upper right panel), IGR J21188+4901 (lower left panel), and IGR J22014+6034 (lower right panel). Black circles with dashed lines (solid blue circles in the online version) indicate the 90% confidence radii of *INTEGRAL* error circle, whereas solid black circles (colored red in the online version) show the positions of the candidate *Chandra* counterparts in these fields given in T12. For each frame, the observed candidates which are presented in this work are labeled with numbers.

(A color version of this figure is available in the online journal.)

Table 2
Chandra Localizations, Counts, Hardness Ratio, and the Probability of Spurious Associations

Candidate No. Chandra Name[a]	R.A.(J2000)	Decl.(J2000)	ACIS Counts	Hardness[b]	P (%)[c]
		IGR J04069+5042			
[1]CXOU J040643.9+504446	$04^h06^m43^s.99$	+50°44′46″.2	5.4	−1.19 ± 1.10	>68
[2]CXOU J040648.7+503931	$04^h06^m48^s.69$	+50°39′31″.2	3.4	−1.30 ± 1.65	>99.99
		IGR J06552−1146			
[1]CXOU J065458.3−114911	$06^h54^m58^s.31$	−11°49′11″.3	8.5	−0.75 ± 0.70	>83
[2]CXOU J065523.6−114601	$06^h55^m23^s.65$	−11°46′01″.1	13.4	−0.62 ± 0.46	33–98
[3]CXOU J065529.5−114900	$06^h55^m29^s.56$	−11°49′00″.1	35.5	+0.02 ± 0.22	14–29
		IGR J21188+4901			
[1]CXOU J211822.9+490627	$21^h18^m22^s.86$	+49°06′26″.7	7.1	−0.78 ± 0.82	>99.96
[2]CXOU J211839.1+485806	$21^h18^m39^s.09$	+48°58′05″.5	4.3	+0.61 ± 1.00	>15
		IGR J22014+6034			
[1]CXOU J220021.1+603342	$22^h00^m21^s.14$	+60°33′41″.8	45.8	−40.91 ± 0.25	>95
[2]CXOU J220109.3+603409	$22^h01^m09^s.34$	+60°34′08″.7	14.4	−0.79 ± 0.46	>88
[3]CXOU J220154.1+603809	$22^h01^m54^s.13$	+60°38′09″.5	31.7	−0.61 ± 0.27	>36
[4]CXOU J220208.4+603042	$22^h02^m08^s.35$	+60°30′42″.4	10.7	−1.15 ± 0.70	>99.99

Notes.
[a] All *Chandra* information is reported by T12.
[b] Hardness ratio is defined as $(C_{2-10\ \mathrm{keV}} - C_{0.3-2\ \mathrm{keV}})/(C_{2-10\ \mathrm{keV}} + C_{0.3-2\ \mathrm{keV}})$ where C is the count rate in the given band. After background subtraction in *Chandra*, the hardness ratios may become negative (T12).
[c] See Equation (1) and T12.

The spectroscopic observations of candidate counterparts for IGR J04069+5042 and IGR J06552−1146 were done at the MDM Observatory, while IGR J21188+4901 and IGR J22014+6034 were observed at TUG.

2.1. TUG Observations

The medium-resolution spectra of the candidate counterparts to the sources IGR J21188+4901 and IGR J22014+6034 were obtained with the TÜBİTAK Faint Object Spectrometer and

Table 3
Observed Possible Optical/IR Counterparts to The Sources

Candidate No. Catalog/Source Name[a]	R.A.(J2000)	Decl.(J2000)	Distances[b]	Magnitudes
		IGR J04069+5042		
[1]2MASS J04064392+5044469	$04^h06^m43^s.92$	$+50°44'46''.95$	$3'.20/1''.00$	$J = 14.40$ $H = 13.68$ $K_s = 13.45$
USNO-A2.0 1500−08672098	$04^h06^m43^s.94$	$+50°44'47''.39$	$3'.23/1''.28$	$B = 18.60$ $R = 16.60$
USNO-B1.0 1505−0322270	$04^h06^m43^s.92$	$+50°44'47''.32$	$3'.21/1''.29$	$B_1 = 19.06$ $R_1 = 16.32$ $B_2 = 18.49$ $R_2 = 16.71$ $I = 15.42$
[2]2MASS J04064872+5039316	$04^h06^m48^s.73$	$+50°39'31''.63$	$2'.76/0''.58$	$J = 11.44$ $H = 11.13$ $K_s = 11.06$
USNO-A2.0 1350−04221566	$04^h06^m48^s.74$	$+50°39'31''.81$	$2'.75/0''.78$	$B = 13.20$ $R = 12.30$
USNO-B1.0 1406−0110577	$04^h06^m48^s.73$	$+50°39'31''.76$	$2'.76/0''.69$	$B_1 = 13.56$ $R_1 = 12.15$ $B_2 = 13.37$ $R_2 = 12.69$ $I = 11.82$
		IGR J06552−1146		
[1]2MASS J06545833−1149119	$06^h54^m58^s.34$	$-11°49'12''.00$	$4'.14/0''.79$	$J = 14.04$ $H = 13.83$ $K_s = 13.32$
USNO-A2.0 0750−03064876	$06^h54^m58^s.35$	$-11°49'11''.80$	$4'.14/0''.74$	$B = 16.60$ $R = 15.40$
USNO-B1.0 0781−0141882	$06^h54^m58^s.33$	$-11°49'11''.89$	$4'.14/0''.64$	$B_1 = 16.95$ $R_1 = 15.43$ $B_2 = 17.48$ $R_2 = 15.34$ $I = 14.60$
		IGR J21188+4901		
[1]2MASS J21182288+4906259	$21^h18^m22^s.89$	$+49°06'25''.96$	$6'.81/0''.78$	$J = 13.01$ $H = 12.45$ $K_s = 12.17$
USNO-A2.0 1350−13821833	$21^h18^m22^s.89$	$+49°06'26''.39$	$6'.82/0''.40$	$B = 18.20$ $R = 16.30$
USNO-B1.0 1391−0394771	$21^h18^m22^s.88$	$+49°06'26''.31$	$6'.82/0''.44$	$B_1 = 18.33$ $R_1 = 16.01$ $B_2 = 18.24$ $R_2 = 16.06$ $I = 14.51$
[2]2MASS J21183906+4858049	$21^h18^m39^s.07$	$+48°58'04''.92$	$3'.27/0''.61$	$J = 14.41$ $H = 13.78$ $K_s = 13.47$
USNO-A2.0 1350−13829476	$21^h18^m39^s.00$	$+48°58'05''.32$	$3'.26/0''.91$	$B = 19.00$ $R = 17.00$
USNO-B1.0 1389−0393707	$21^h18^m39^s.06$	$+48°58'05''.28$	$3'.26/0''.37$	$B_1 = 18.57$ $R_1 = 17.12$ $B_2 = 18.66$ $R_2 = 16.69$ $I = 15.91$
		IGR J22014+6034		
[1]2MASS J22002116+6033420	$22^h00^m21^s.17$	$+60°33'42''.06$	$8'.09/0''.34$	$J = 11.66$ $H = 10.99$ $K_s = 10.82$
USNO-A2.0 1500−08655368	$22^h00^m21^s.17$	$+60°33'42''.11$	$8'.09/0''.38$	$B = 15.50$ $R = 13.7$
USNO-B1.0 1505−0321733	$22^h00^m21^s.27$	$+60°33'42''.44$	$8'.08/1''.13$	$B_1 = 15.41$ $R_1 = 13.61$ $B_2 = 15.19$ $R_2 = 13.38$ $I = 12.29$
[2]2MASS J22010934+6034088	$22^h01^m09^s.34$	$+60°34'08''.81$	$2'.17/0''.11$	$J = 10.62$ $H = 10.39$ $K_s = 10.32$
USNO-A2.0 1500−08672098	$22^h01^m09^s.29$	$+60°34'08''.12$	$2'.18/0''.67$	$B = 12.70$ $R = 11.00$
USNO-B1.0 1505−0322270	$22^h01^m09^s.28$	$+60°34'08''.00$	$2'.18/0''.82$	$B_1 = 12.57$ $R_1 = 11.00$ $B_2 = 11.72$ $R_2 = 10.86$ $I = 10.69$
[3]2MASS J22015416+6038094	$22^h01^m54^s.16$	$+60°38'09''.48$	$5'.33/0''.23$	$J = 11.50$ $H = 11.11$ $K_s = 10.94$
USNO-B1.0 1506−0321404	$22^h01^m53^s.99$	$+60°38'09''.60$	$5'.32/1''.02$	$B_1 = 14.59$ $R_1 = 11.77$ $B_2 =$ - $R_2 = 12.46$ $I = 11.74$
[4]2MASS J22020837+6030425	$22^h02^m08^s.37$	$+60°30'42''.50$	$6'.06/0''.18$	$J = 12.59$ $H = 11.95$ $K_s = 11.71$
USNO-A2.0 1500−08693376	$22^h02^m08^s.28$	$+60°30'42''.83$	$6'.05/0''.68$	$B = 17.50$ $R = 15.50$
USNO-B1.0 1505−0322924	$22^h02^m08^s.38$	$+60°30'42''.77$	$6'.06/0''.43$	$B_1 = 17.37$ $R_1 = 15.27$ $B_2 = 17.19$ $R_2 = 15.38$ $I = 13.54$

Notes.
[a] The catalogs are the Two Micron All Sky Survey (2MASS; Cutri et al. 2003) and the United States Naval Observatory (USNO-B1.0 and USNO-A2.0, Monet 1998, 2003). The astrometric accuracy of 2MASS and USNO catalogs are $\leqslant 0''.1$ (Skrutskie et al. 2006) and $0''.2$, respectively (Deutsch 1999; Assafin et al. 2001; Monet 2003).
[b] The angular distance from the center of the *INTEGRAL* error circle/the angular distance from the *Chandra* position reported by T12.

Camera which is mounted on the Russian–Turkish 1.5 m Telescope (RTT150) located at TUG, Antalya, Turkey. The camera is equipped with a 2048 × 2048, 15 μm pixel Fairchild 447BI CCD. It has an FOV of $13' \times 13'$ with a pixel scale of $0''.39$ pixel^{-1}. Grism 15, having an average dispersion of 3 Å pixel^{-1}, and slit 67 μm ($1''.24$) were used providing a 3300–9000 Å wavelength band.

All spectroscopic data, acquired on 2011 August 27 under good weather conditions, were reduced using the Long-Slit package of MIDAS[11] to obtain one-dimensional spectra of target sources. The spectra were corrected for bias, flat-fielded and cleaned from the cosmic-ray hits with standard MIDAS routines. Wavelength calibration of the spectra were done by Neon lamp spectrum. The heliocentric correction was applied to each spectrum after the extraction was done. The spectrophotometric standard star BD +33°2642 (Oke 1990) was observed during the observing night to get the flux-calibrated spectra of the candidate counterparts.

The equivalent widths (EW) of prominent absorption and emission lines are measured by the ALICE subroutine of MIDAS.

2.2. MDM Observations

We used the Ohio State Multi-Object Spectrograph with the MDM4K CCD on the 2.4 m Hiltner Telescope of the MDM Observatory on 2011 January 11 and 13. The Volume Phase Holographic transmission grating we utilized has a $1''.2$ wide slit with a wavelength coverage of 3900–6800 Å at 3.5 Å resolution. Conditions were clear during the observing runs. Spectra of two *Chandra* localized X-ray sources in the *INTEGRAL* error circle of IGR J04069+5042, and of one X-ray source for IGR J06552−1146 were obtained. The spectral reduction was performed using standard IRAF[12] routines. The flux calibration was done by Oke & Gunn (1983) standard stars. We also obtained images in the *R* band using the same CCD for sources that are not in the standard catalogs.

[11] http://www.eso.org/projects/esomidas/

[12] http://iraf.noao.edu/

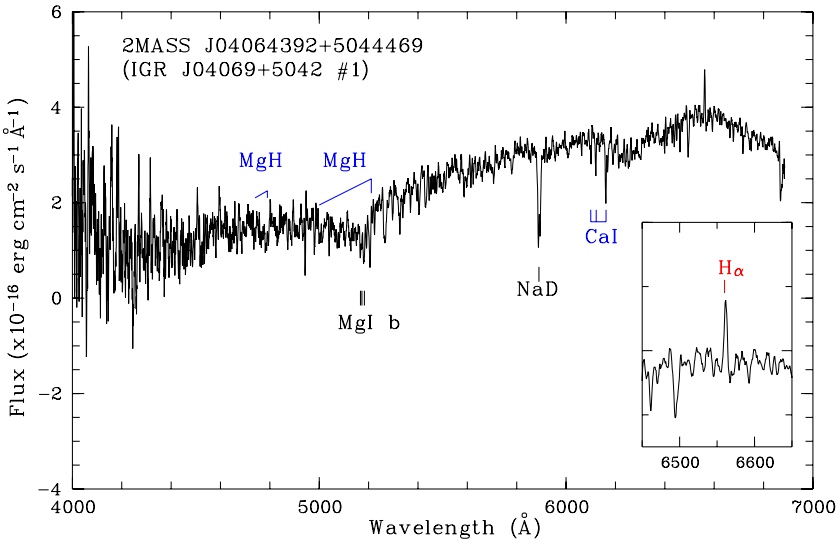

Figure 2. Spectrum of candidate 1 of IGR J04069+5042. A weak Hα emission line can be distinguished from the noise level. This source is identified as a K5–7-type main-sequence star due to the existence of molecular MgH bands and the similarities between the stars of the same spectral type.

(A color version of this figure is available in the online journal.)

Table 4
EW Measurements of Candidate Counterparts to IGR J04069+5042 and IGR J06552−1146

		IGR J04069+5042		IGR J06552−1146
		J04064392+5044469	J04064872+5039316	J06545833−1149119
Sr II	λ4077	...	0.65 ± 0.11	...
Hδ		...	2.42 ± 0.18	...
Ca I	λ4226	...	0.94 ± 0.13	...
Hβ		...	2.8 ± 0.23	
Ca I triplet	λ6103	0.53 ± 0.06	<0.07	0.56 ± 0.04
	λ6122	1.00 ± 0.04	<0.05	0.98 ± 0.14
	λ6162	1.95 ± 0.30	<0.3	1.42 ± 0.20
Hα		−1.07 ± 0.04	2.41 ± 0.08	−0.45 ± 0.05
Spectral Class		K5–7 Ve	F5–8 III–V	K5–8 Ve

Note. EW measurements are given in Å units and by convention, positive values denote the absorption lines.

2.3. Chandra Observations

We used the *Chandra* observations not only for determining optical counterpart candidate positions, but also obtaining soft X-ray properties which could aid in the identification process. We fitted the *Chandra* 0.3–10 keV spectra with an absorbed power-law model to determine the absorbed 0.3–2 keV and 2–10 keV flux for each source. We defined the hardness ratio as $(F_{2-10\ \mathrm{keV}} - F_{0.3-2\ \mathrm{keV}})/(F_{2-10\ \mathrm{keV}} + F_{0.3-2\ \mathrm{keV}})$. For details of spectral fitting, background subtraction, and flux calculation, see T12. For soft X-ray properties relevant for this work, see Table 2.

3. RESULTS

3.1. IGR J04069+5042

We performed optical spectroscopy of two possible candidates localized by *Chandra* within the *INTEGRAL* error circle of 4.′2.

2MASS J04064392+5044469 (1). The optical spectrum includes prominent absorptions of Na I D resonance lines, Mg I b and Ca I triplet lines (see Figure 2). Although distinguishing features in the classification region are mostly at the noise level, the spectrum is very similar to the K-type main-sequence star HD 283916 (SAO 76803) in Jacoby et al. (1984) and to the sources within the same class in Ross et al. (1996). Indeed, the presence of MgH bands at around λ4780 and λ5200, seen only in the spectra of main-sequence stars, supports the luminosity classification. On the other hand, a weak but noticeable Hα emission line (EW = 1.07 Å; see Table 4) which could be due to the chromospheric activities, stellar winds, and/or interactions with the environment of the secondary (or primary) indicates an active star. Therefore, we classify this source as a K5–7 Ve-type star based on its spectral lines and EW measurements.

2MASS J04064872+5039316 (2). The spectrum is dominated by neutral hydrogen lines (Hδ, Hγ, Hβ, and Hα) and several metallic lines of Fe I, Sr II, Mg I, and Mg II (see Figure 3). The Ca I triplet lines that are used as luminosity indicators are very weak (see Table 4) as seen in the spectra of F-type stars (Montes & Martín 1998; Cayrel et al. 1996). In addition, the *G* band of CH at λ4300 that becomes visible for the spectral types later than F4 and increases in strength with decreasing temperature (Gray & Corbally 2009) is one of strongest features in the blue region (4000–5000 Å) and allows us to exclude the earlier spectral classes. Comparing the line width ratio of λ4077 (Sr II) to λ4226 (Ca I) that is a sensitive criteria for luminosity (Morgan et al. 1943), and the EW measurements of Balmer lines (see Table 4) to the values in Jaschek

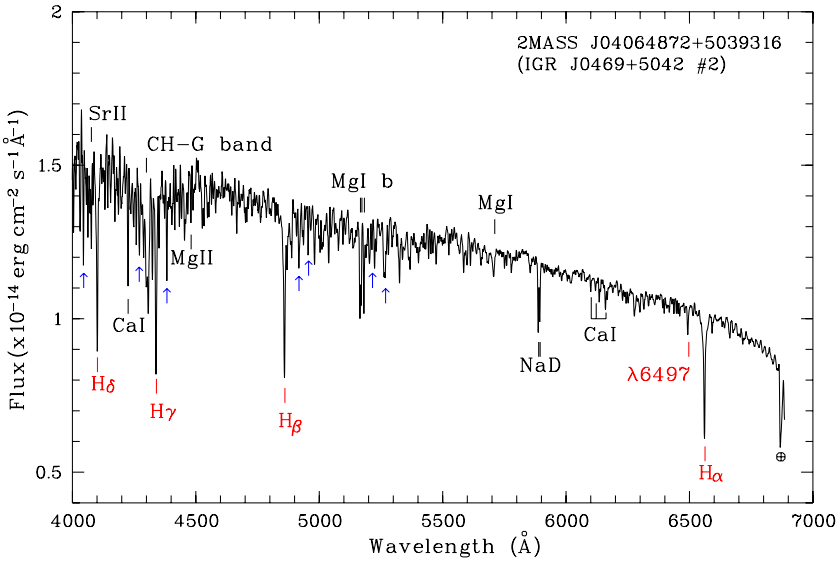

Figure 3. Spectrum of candidate 2 of IGR J04069+5042 shows the characteristics of an F-type star. Black arrows (colored blue in the online version) indicate the Fe I lines at λλ4046, 4271, 4383, 4819, 4957, 5216, and 5270, respectively, whereas symbol ⊕ shows the telluric absorption band. The Balmer series lines and the CH-G band are the most prominent features. Neutral and singly ionized magnesium lines, Ca I triplet, NaD absorption, and the blend of several metal lines at 6497 Å are also visible.

(A color version of this figure is available in the online journal.)

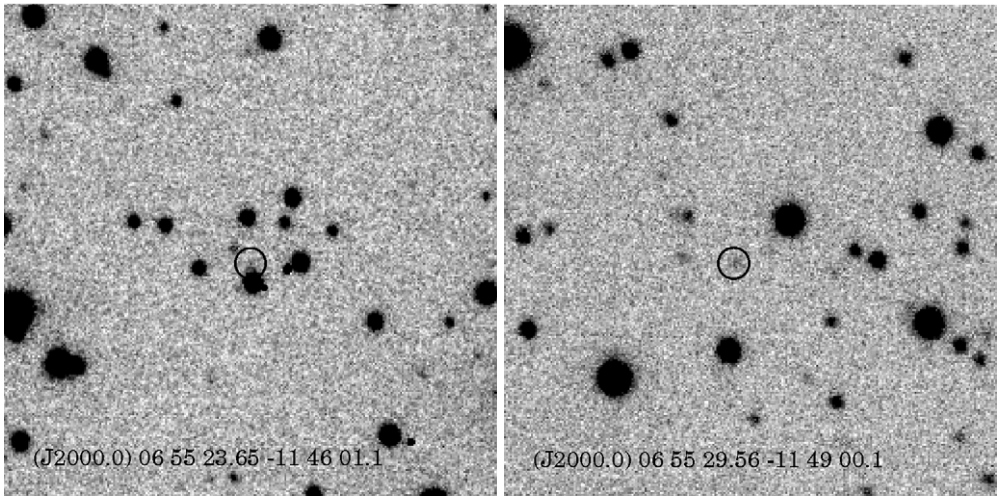

Figure 4. *R*-band images of the field around the candidates 2 (left panel) and 3 (right panel) of IGR J06552−1146. The black circles show the positions of *Chandra* sources, but the radii are larger than the error radii for clarity. The *Chandra* error radii are 0.″68 and 0.″81, respectively. For candidate 2, the source in the error circle is ambiguous while the *Chandra* position is not coincident with any optical or IR counterpart in the catalogs for the latter. The *R*-band magnitude of the weak source in the error circle for the candidate 3 is found to be 22.17 ± 0.14 from the aperture photometry.

& Jaschek (1995) and in Eaton (1995), we suggest that this source could be an F5–8-type star within the luminosity class of III–V.

3.2. IGR J06552−1146

Optical spectroscopy was only obtained for candidate 1 (see Figure 1) which is ∼0.″8 away from its *Chandra* counterpart. Candidate 2 is 2.″8 away from the nearest source in 2MASS and USNO catalogs. As it can also be seen in the *R*-band image of this source (Figure 4), the *Chandra* source cannot be clearly identified with an optical counterpart. Likewise, candidate 3 was not listed in Table 1 since its coordinates are not associated with any optical or IR counterparts in the catalogs. However, a weak source in the *Chandra* error circle is visible in the *R*-band image of the field (Figure 4). This source has an *R* magnitude of 22.17 ± 0.14.

2MASS J06545833−1149119 (1). The flux-calibrated spectrum of candidate 1 shows Fe I, Mg I, and Ca I absorption lines (see Figure 5) and a weak (EW = 0.45 Å) Hα emission line (see Table 4). The characteristics of the spectrum are very similar to those of candidate 1 to IGR J04069+5042 in terms of the existence of the spectral lines and the molecular MgH band. To give a spectral range, we searched the spectral atlases and libraries having a similar spectrum to that of 2MASS J06545833−1149119. By comparing the spectra of the sources listed in Jacoby et al. (1984), Ross et al. (1996), and in Gray & Corbally (2009) to candidate 1, we suggest that it would be a main-sequence K5–8-type emission-line star.

3.3. IGR J21188+4901

This source is tentatively classified as a transient in Bird et al. (2010) due to its highly variable X-ray flux in 20–40 keV

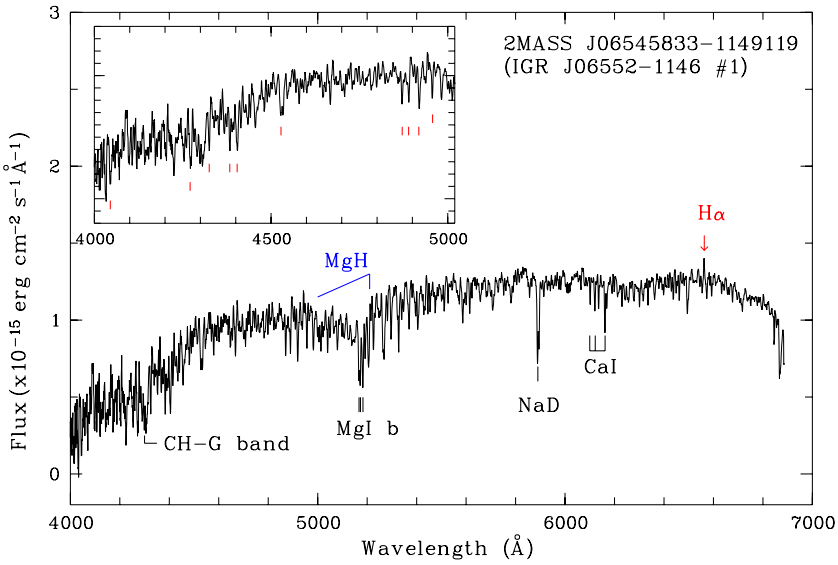

Figure 5. Flux-calibrated spectrum of candidate 1 to IGR J06552−1146. Fe I lines at λλ4046, 4271, 4325, 4383, 4404, 4528, 4871, 4889, 4918, 4957 are represented by small black bars (colored red in the online version) in a separate panel for clarity. A weak Hα emission is also seen in the main panel.
(A color version of this figure is available in the online journal.)

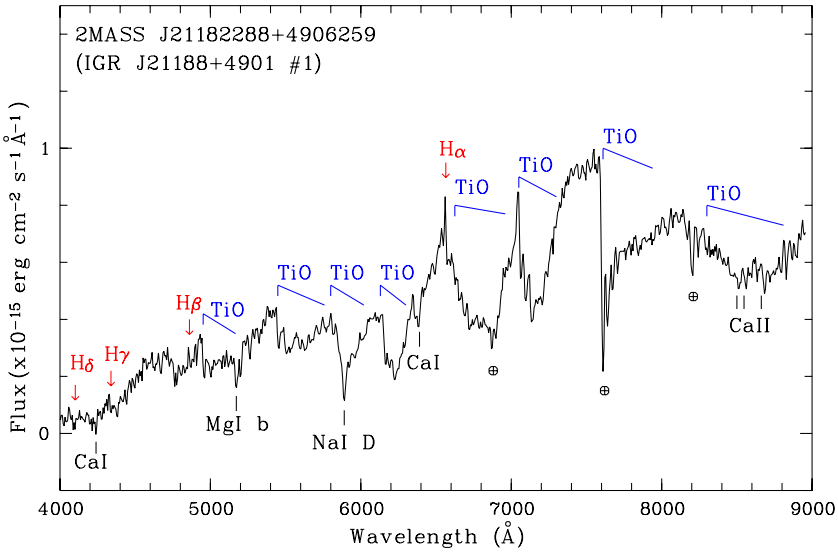

Figure 6. Identified features in flux-calibrated spectrum of candidate 1 to IGR J21188+4901. The spectrum contains both broad molecular TiO bands with a red continuum and a prominent Hα emission, indicating an M-type chromospherically active star. The telluric absorption bands are denoted by ⊕ symbol.
(A color version of this figure is available in the online journal.)

energy band. Two candidates which are quite faint in the optical band have been observed (Figure 1) to search for the optical counterpart to IGR J21188+4901.

2MASS J21182288+4906259 (1). The optical spectrum of this source contains both broad molecular TiO bands with a red continuum and an Hα emission line with EW = 1.9 Å. Although EW values of Hγ and Hβ lines could not be determined due to their low signal to noise, they are apparent in emission. These spectral features are indicative of a late-type star spectrum with chromospheric activity. Ca I and Ca II triplet lines, used as a luminosity indicator for M-type stars (Jaschek & Jaschek 1995), Mg I lines and telluric absorption bands are the other identified features in the spectrum (see Figure 6). We point out that the spectral appearance of this candidate is very similar to that of the counterparts of 1RXS J174607.8−213333 and IGR J11098−6457 which are identified as an M2–4 (Masetti et al. 2008) and an M2-type (Masetti et al. 2009) symbiotic giants, respectively. However, this source does not have the clear spectral features of a red giant star. In addition, 2MASS magnitudes are too faint to be a nearby giant. Therefore, we searched for the late-type stars spectra in the atlases of Gunn & Stryker (1983), Jacoby et al. (1984), and Silva & Cornell (1992) to compare with our flux-calibrated spectrum and we determine that the spectral class of this candidate could be an M3–5-type active main-sequence star.

2MASS J21183906+4858049 (2). This candidate is the only source having a *Chandra* counterpart within the *INTEGRAL* error circle. The spectrum shown in Figure 7 has typical features of a late-K/mid-M-type star (Gray & Corbally 2009) without any emission lines. In addition, the molecular CaOH band that becomes visible for dwarfs having spectral class later than K7 and MgH bands are prominent features in the spectrum. The weakness and/or absence of the Balmer lines (see Table 5) support the late-type spectral classification. Therefore,

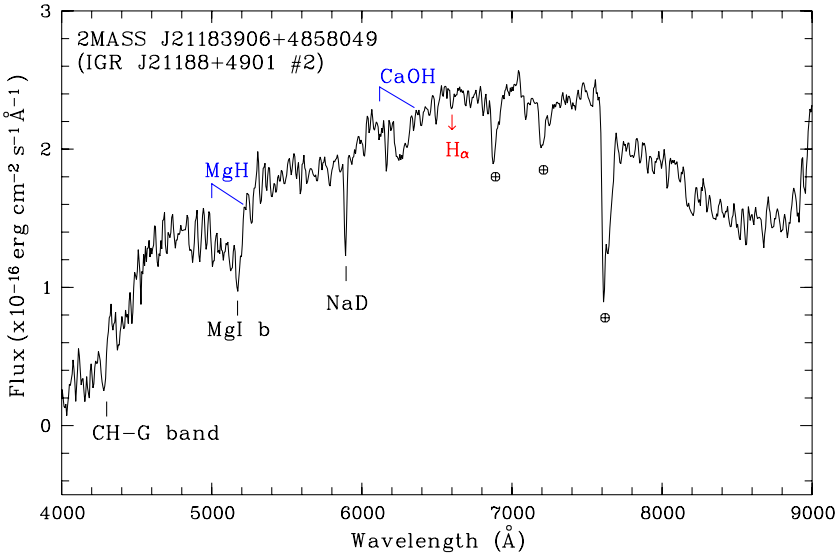

Figure 7. Flux-calibrated spectrum of candidate 2 to IGR J21188+4901. The source has typical features of a late-type star. The symbol ⊕ indicates the telluric absorption bands.

(A color version of this figure is available in the online journal.)

Table 5
EW Measurements of Counterparts to IGR J21188+4901 and IGR J22014+6034

		IGR J21188+4901			
			J21182288+4906259	J21183906+4858049	
Hα			−1.9 ± 0.24	<0.03	
Spectral Class			M3–5 Ve	K7–M4 V	
		IGR J22014+6034			
		J22002116+6033420	J22010934+6034088	J22015416+6038094	J22020837+6030425
Ca II H & K	λ3934	−1.02 ± 0.51	...	...	...
	λ3968	−1.36 ± 0.07	...	...	...
Hβ		...	4.22 ± 0.01	...[a]	...
Fe I	λ5269	...	1.07 ± 0.01	...	...
Hα		−2.15 ± 0.03	3.60 ± 0.01	2.26 ± 0.01	−3.8 ± 0.05
Ca II triplet	λ8498	...	1.82 ± 0.05	1.25 ± 0.04	...
	λ8542	...	2.49 ± 0.03	2.42 ± 0.02	...
	λ8662	...	2.01 ± 0.01	2.36 ± 0.01	...
Spectral class		K7–M4 Ve	F5–G5 III–V	G III–IV	M2–5 Ve

Notes. EW measurements are given in Å units and, by convention, positive values denote the absorption lines.
[a] Since Hβ absorption of J22015416+6038094 is highly blended, its EW measurement is not given in the table.

considering characteristics of the spectrum, we suggest a K7–M4-type main-sequence classification for this source.

3.4. IGR J22014+6034

We obtained optical spectroscopy of four stars that are detected with *Chandra* in 2MASS and USNO catalogs. Two of these candidate optical/IR counterparts lie within the 5′.4 radius *INTEGRAL* error circle as seen in Figure 1.

2MASS J22002116+6033420 (1). The flux-calibrated spectrum is very similar to candidate 2 of IGR J21188+4901 that is classified as a K7–M4-type main-sequence star. It is dominated by the molecular MgH, CaOH, and CH-G bands in addition to Mg I b triplet lines (see Figure 8). The emission lines of Hα and Ca II H & K at λ3968, λ3934 (see Table 5), indicators of chromospheric activity, are also detected.

2MASS J22010934+6034088 (2). This IR source is the optically brightest candidate to the X-ray position of IGR J22014+6034. However, the optical spectrum contains no significant features related to an X-ray source. The most prominent absorptions in the blue region of the spectrum are of Ca II H & K and Balmer series lines. Metallic lines of Fe I and Mg I b triplet are also visible. The flux-calibrated spectrum of 2MASS J22010934+6034088 is similar to that of A–G-type stars due to its decaying blue continuum toward the longer wavelengths (see Figure 9). On the other hand, the presence of CH-G band and the weakness of Balmer lines (see Table 5) while compared to A-type stars indicate that this source must be in the F–G spectral range. By comparing EW values of Ca II triplet lines in near IR region to those of late-type stars (Jaschek & Jaschek 1995; Zhou 1991), we classify this candidate as an F5–G5-type III-V star.

2MASS J22015416+6038094 (3). This bright IR star is located at edge of the IGR error circle. It does not have an optical counterpart in USNO-A2.0 catalog. Although the flux-calibrated spectrum contains nearly most of the features detected

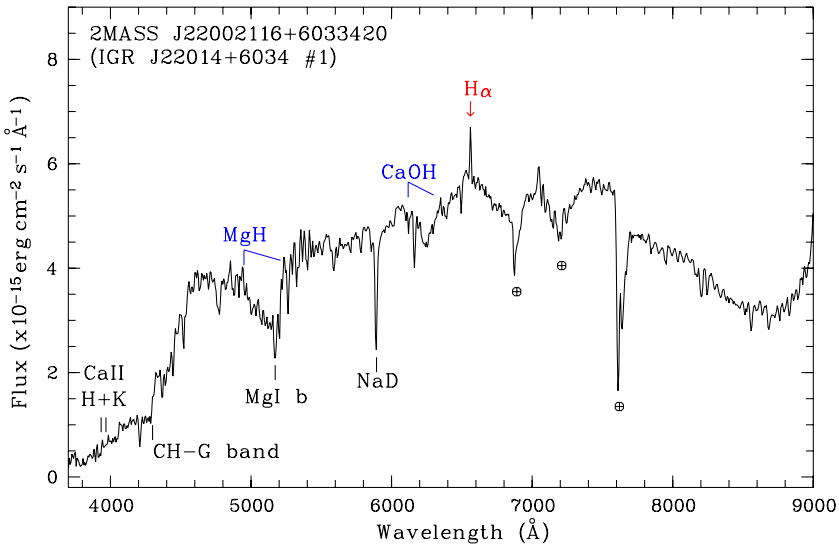

Figure 8. Flux-calibrated spectrum of candidate 1 to IGR J22014+6034. The emission lines of Ca II H & K and Hα can be considered as indicators of a chromospherically active star.

(A color version of this figure is available in the online journal.)

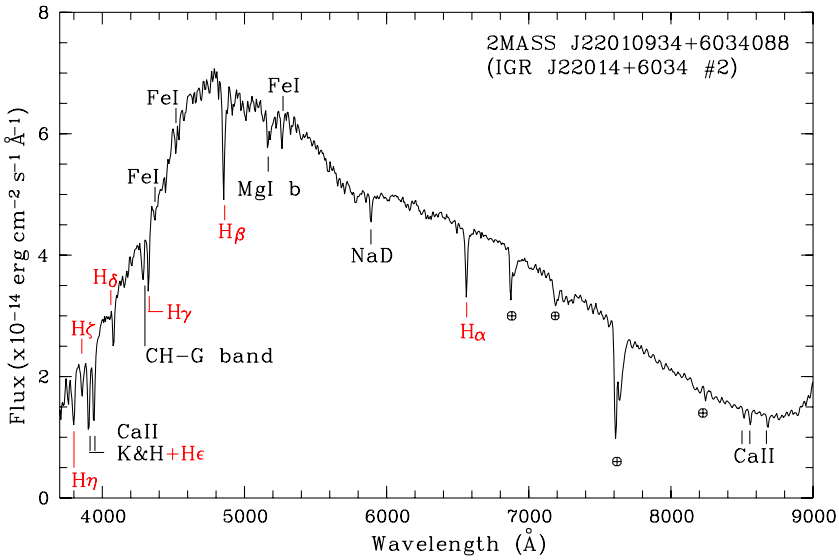

Figure 9. Flux-calibrated spectra of 2MASS J22010934+6034088, candidate 2 to IGR J22014+6034. The spectrum is dominated by Balmer series lines and metallic lines of Fe I, Mg I. The symbol $\oplus$ denotes the atmospheric telluric bands.

(A color version of this figure is available in the online journal.)

in 2MASS J22010934+6034088, they are different regarding the strength of the lines (see Table 5). The identification spectrum of candidate 3 is shown in Figure 10. The Balmer lines of Hδ and Hγ are extremely weak or absent, compared to Hα line (EW = ~2.3 Å) and to CH-G band. The blue region of the spectrum, which is dominated by metallic lines of Mg I, Mg II, and Fe I, displays typical spectral features of a late-type star. We derive a spectral class of G III–IV based upon the prominent features for this source.

2MASS J22020837+6030425 (4). The coordinates of the source are coincident with the positions of USNO-B1.0 1505−0322924 and USNO-A.2 1500−08693376 although they fall just outside the *INTEGRAL* error circle (6.′06). The flux-calibrated 4000–9000 Å spectrum shows typical features of an M-type star (see Figure 11) dominated by strong molecular bands of TiO (Gray & Corbally 2009). The emissions of Balmer series lines (Hγ, Hβ, Hα) superposed with TiO bands and the presence of Ca I, Ca II, Mg I b lines are in favor of the late-type spectral classification (see Table 5). Since determining exact spectral class of late-type stars is rather complicated due to the contaminated blue part of the spectrum, we used spectrophotometric atlases of Gunn & Stryker (1983), Jacoby et al. (1984), and the library of Silva & Cornell (1992) to secure the spectral and luminosity classification. Comparing our spectrum with the late-type stars in the atlases and libraries we classify 2MASS J22020837+6030425 as a main-sequence M2–5-type chromospherically active star.

3.5. X-Ray Results

The four IGR sources we investigated in this work are reported as sources for which none of the *Chandra* sources in the FOV stands out as a candidate counterpart from a likelihood analysis soley based on X-rays as described in T12.

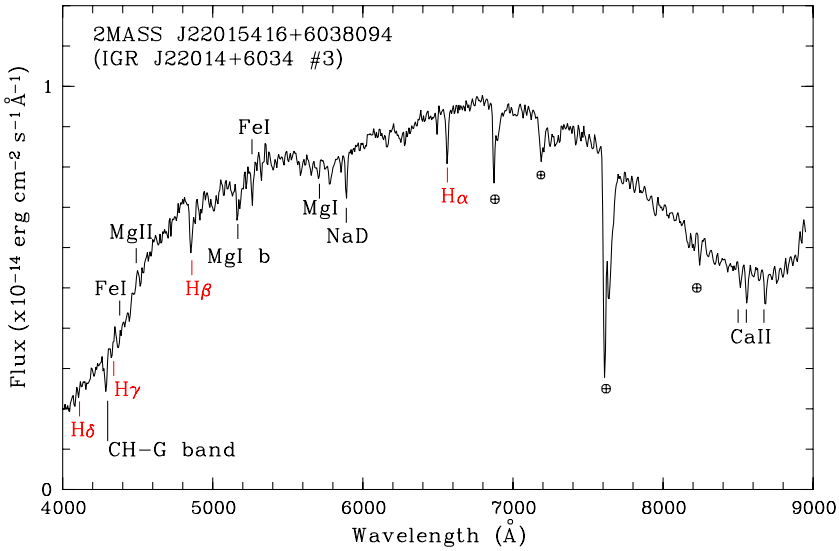

Figure 10. Flux-calibrated spectrum of 2MASS J22015416+6038094, candidate 3 to IGR J22014+6034. The main spectral features Mg I, Mg II, and Fe I lines in addition to Balmer series lines are labeled. The symbol ⊕ denotes the atmospheric telluric bands. This candidate is identified as a G-type star.

(A color version of this figure is available in the online journal.)

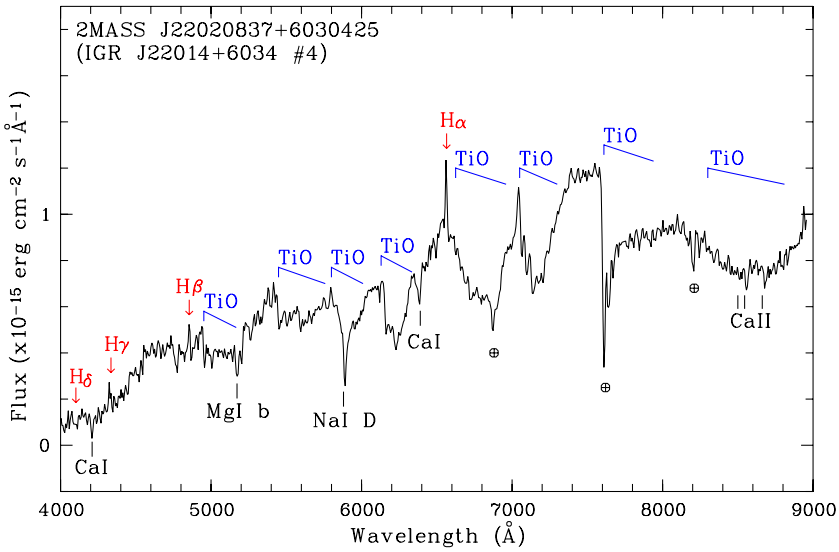

Figure 11. Flux-calibrated spectrum of candidate 4 to IGR J22014+6034. The spectrum shows typical spectral features of an M-type main-sequence star dominated by strong molecular bands of TiO.

(A color version of this figure is available in the online journal.)

This likelihood analysis calculates the spurious association probability as

$$P = 1 - e^{-N(>F_{2-10\ \mathrm{keV}})\,\pi\,\theta^2_{\mathrm{search}}}, \quad (1)$$

where $N(>F_{2-10\ \mathrm{keV}}) = 9.2\ (F_{2-10\ \mathrm{keV}}/10^{-13})^{-0.79}\ \mathrm{deg}^{-2}$ (Sugizaki et al. 2001, T12), and $F_{2-10\ \mathrm{keV}}$ is the absorbed 2–10 keV flux in erg cm^{-2} s^{-1}. θ_{search} is the radius of the search region in units of degrees and equals 90% confidence for the sources inside the *INTEGRAL* error circle (see Table 1). For sources outside the error circle, it indicates the angular separation from the center of the *INTEGRAL* error circle. The spurious association probabilities of all sources are given in Table 2.

For most of the candidates, the spurious association probability is very high. The notable exceptions are candidate 3 of IGR J06552−1146, candidate 2 of IGR J21188+4901, and candidate 3 of IGR J22014+6034. However, the likelihood analysis does not take into account the variability. The soft X-ray measurements were obtained at an arbitrary epoch, and *INTEGRAL* analysis shows that the maximum hard X-ray flux and the average hard X-ray flux are different for these sources, indicating variability (see Table 1; T12; Bird et al. 2010). In fact, IGR J04069+5042 and IGR J06552−1146 have bursticity[13] impact grater than 1.1 and for IGR J21188+4901 it is greater than 4, indicating a highly variable nature of the source in X-rays (Bird et al. 2010). Therefore, likelihood analysis based on X-ray data alone may fail in revealing the true counterpart if the X-ray observations take place when the source is weak. It is still possible that one of the detected *Chandra* sources is the correct counterpart.

[13] Bursticity can be defined as the ratio of the maximum significance on any timescale, compared to the average significance (Bird et al. 2010).

4. DISCUSSION

Below, we discuss the candidate counterparts for each IGR source in terms of their optical spectra, *Chandra* soft X-ray properties, and relative probabilities to find out the candidates that are more likely to be the IGR source.

4.1. IGR J04069+5042

According to Equation (1), the spurious association probabilities of candidates 1 and 2 are >68%, and >99.99%, respectively, and neither of them was detected in the 2–10 keV band with *Chandra*. Among these two sources, candidate 2 has typical features of a late F-type star. On the other hand, candidate 1 shows H_α emission, which makes it more likely to be the correct counterpart.

4.2. IGR J06552−1146

Candidate 1 is 4.′14 away from the center of the *INTEGRAL* error circle and the probability of spurious association is 88%. The spectrum shows evidence of an H_α emission line and it is similar to that of candidate 1 for IGR J04069+5042. The other sources with high ACIS count rates are too dim in the optical to get a spectrum. Their spurious association probabilities are 33%–98% and 14%–29% for candidates 2 and 3, respectively. Candidate 3 in fact has positive hardness ratio, and the relative probability is quite close to the cutoff for a *Chandra*/*INTEGRAL* association in T12.

4.3. IGR J21188+4901

Candidate 1 is outside the 90% confidence error circle of *INTEGRAL* with spurious association probability of >99.96%. It has been detected with *Chandra* in the 2–10 keV band, and is an active M-type star. Candidate 2 is the only soft X-ray source (detected in 0.3–2 keV energy band) in the *INTEGRAL* error circle with a probability of >15%, but it is not detected with *Chandra* in the 2–10 keV band. Candidate 2 shows properties of a late-type (K7–M4) main-sequence star. Based on probabilities, candidate 2 is a more likely counterpart than candidate 1.

4.4. IGR J22014+6034

The first candidate is the brightest *Chandra* source in the vicinity of the IGR source, however, it is out of the 90% confidence error circle of *INTEGRAL*. The spectrum is typical of an active late-type star. The probability of spurious association is >95% and it is detected in the 2–10 keV band with *Chandra*, however, the source is very soft.

The optical spectra of candidates 2 and 3 show that they are late-type main-sequence stars without emission lines. The probabilities of spurious associations for these sources are >88% and >36%, respectively.

The optical spectrum of candidate 4 shows features of an active M-type main-sequence star. It is located just outside the error circle of *INTEGRAL*. The probability is >99.98%, and it is not detected with *Chandra* in the 2–10 keV band.

4.5. IGR Sources Identified as Symbiotic Systems

At an early phase of our analysis, we compared our optical spectra with those published in Masetti et al. (2008, 2009, 2012) and realized the similarities of candidate 1 of IGR J21888+4901 and candidate 4 of IGR J22014+6034, the M-type stars with broad TiO bands, to those identified as symbiotic stars. However, these sources do not show He I, He II, and [O III] in emission

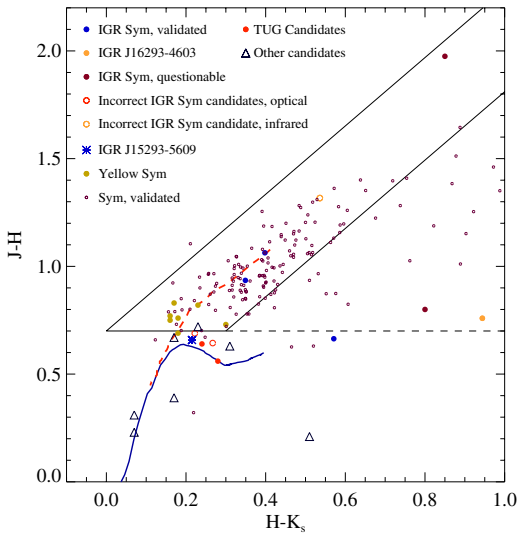

Figure 12. $H-Ks$ vs. $J-H$ diagram for all sources discussed in this work. The validated symbiotics are taken from Phillips (2007), and shown with small, empty, gray circles (colored purple in the online version). The black solid lines enclose the S-type symbiotics, whereas the single dashed line and the first solid line enclose D-type symbiotics (Corradi et al. 2008). The locus of points for main-sequence stars and red giant branch stars are represented by a black solid line (colored blue in the online version) and a gray dashed line (colored red in the online version), respectively. The questionable symbiotic counterparts (diamonds, colored brown in the online version) are for IGR J16358−4726, IGR J17497−2821, and 1RXS J174607.8-213333, the incorrect IGR symbiotic candidates (empty black circles, colored red in the online version) are for IGR J11098−6457 and IGR J17197−3010, and the incorrect IGR symbiotic identified through *K*-band spectroscopy is for IGR J16393−4643. See Section 4.5 for more details.

(A color version of this figure is available in the online journal.)

(Kenyon 1986), and their infrared colors are not consistent with the colors of symbiotics in the $J-H$ versus $H-Ks$ diagram as given by Phillips (2007) and Corradi et al. (2008). Our candidates are more likely active main-sequence stars e.g., dMe stars (Pettersen & Hawley 1989) rather than giants. To illustrate this we plotted the NIR color–color diagram of M-type TUG candidates (empty, black circles with crosses, filled red circles in the online version) along with colors of several other sources in Figure 12. The plot includes validated IGR symbiotics (IGR J10109−5746, IGR J12349−6434, and IGR J16194−2810 with filled black circles; colored blue in the online version) and the all known symbiotics (small, empty, gray circles; colored purple in the online version), the boundaries that limit stellar (S)- and dusty (D)-type symbiotics (see Pereira & Roig 2009 for details of S- and D-type symbiotics) and the loci of main-sequence stars and red giant stars. The colors of IGR sources, tentatively classified as symbiotic systems but later shown to have the incorrect counterpart candidates, are also placed in Figure 12. The initial classifications of the counterparts to IGR J11098−6457, IGR J17197−3010 (empty black circles; colored red in the online version), and IGR J16393−4643 (empty gray circle, colored orange in the online version) were done with optical and/or IR spectral analyses. Since the refined X-ray positions of these IGR sources were not related to the suggested counterparts, the symbiotic identifications were ruled out. Note that the colors of incorrect counterparts can easily be associated with the main-sequence stars like the TUG candidates.

Two other candidates were also tentatively claimed to be symbiotic binaries, IGR J16358−4726, IGR J17497−2821, but subsequent analyses made the symbiotic interpretation questionable

Table 6
Summary Table

$^{Candidate\,No.}$Chandra Name	Spectral Class	Type	Notes
		IGR J04069+5042	
[1]CXOU J040643.9+504446	K5–7 Ve	Active star; RS CVn?	Hα emission, lower SAP[a]
[2]CXOU J040648.7+503931	F5–8 III–V	Late-type star	No emission lines, higher SAP
		IGR J06552−1146	
[1]CXOU J065458.3−114911	K5–8 Ve	Active Star; RS Cvn?	Hα emission, higher SAP
[2]CXOU J065523.6−114601	...	?	No optical spectrum, intermediate SAP
[3]CXOU J065529.5−114900	...	?	No optical spectrum, low SAP, positive hardness
		IGR J21188+4901	
[1]CXOU J211822.9+490627	M3–5 Ve	Active Star; Flare star?	Hα emission, higher SAP
[2]CXOU J211839.1+485806	K7–M4 V	Late-type star	lower SAP but not detected in 2–10 keV
		IGR J22014+6034	
[1]CXOU J220021.1+603342	K7–M4 Ve	Active star	Hα emission, high SAP, detected in 2–10 keV
[2]CXOU J220109.3+603409	F5–G5 III–V	Late-type star	No features, high SAP
[3]CXOU J220154.1+603809	G III–IV	Late-type star	No features, lower SAP
[4]CXOU J220208.4+603042	M2–5 Ve	Active star; Flare star?	Hα emission, higher SAP

Note. [a] SAP: Spurious Association Probability.

(see Introduction for details). Moreover, the identification of 1RXS J174607.8-213333 (Masetti et al. 2008) relied online on low-resolution optical spectrum which requires further analysis. As mentioned in Masetti et al. (2008), it could be a spurious detection. These sources are shown as "IGR Sym, questionable" in Figure 12 (Diamonds, colored brown in the online version). The colors of the infrared counterpart of IGR J16293−4603 (filled gray circle with a cross, filled orange circle in the color online version) are also consistent with being a symbiotic system as expected, since the initial identification was done using *g*, *r*, and *i* colors by Ratti et al. (2010). We also show IGR J15293−5609, classified as a symbiotic with a *K*-type companion (balck star, colored red in the online version). This source falls slightly out of the region of validated symbiotics. On the other hand, symbiotics with *K*-type companions are rare, and occupy lower $J-H$ values (Pereira & Roig 2009) just like IGR J15293−5609. These are called yellow symbiotic systems which are indicated separately in Figure 12 (filled, gray circles, colored dark yellow in the online version). We also note that reddening can move the sources along the diagonal lines shown in the figure, and the large uncertainty in A_V of IGR J15293−5609 (T12) could easily move this source to the confirmed region. Finally, we show the colors of all other candidates that we identify as main-sequence stars (with triangles), and as expected most of them lie along the locus of main-sequence stars.

This analysis shows that near infrared color diagram provides a quick method to double check identifications of symbiotics with some caveats. First of all, many symbiotic systems have normal NIR colors (see confirmed symbiotics, and the locus of red giant branch stars in Figure 12). NIR colors may be enough to claim a giant identification, but it does not mean that the system is a symbiotic. Second, most Galactic IGR sources are in the plane with high extinction (including the sources we analyzed, all with $A_V > 3$) which could move main-sequence stars into the range of symbiotics.

5. CONCLUSIONS

We tabulate the properties of all of the investigated sources in Table 6. We found several chromospherically active late-type stars that might be the counterparts of the IGR sources. A special type of active stars, the RS CVn systems, significantly contribute to the population of X-ray sources above 2 keV (Motch et al. 2010). After the tentative identification of IGR J08023−6954 as an RS CVn system by Rodriguez et al. (2010), two more IGR sources were identified in this class of binaries with active coronae (Masetti et al. 2012). These sources are variable in hard X-rays (Barbier et al. 2005; Osten et al. 2007), and therefore can be detected with *INTEGRAL*. Given the similarity of the optical spectra, candidate 1 of IGR J04069+5042 or candidate 1 of IGR J06552−1146 may be RS CVn if either of them is the actual counterpart.

The total number of IGR systems claimed to be symbiotics is eight. Including IGR J15293−5746, the number of multiple method confirmed symbiotics is four. For our candidates with deep TiO bands, we cannot confirm the symbiotic nature as their near infrared colors are not consistent with known symbiotics. Given that the active dMe stars are ubiquitous in our Galaxy, some of the suggested counterparts to the IGR sources claimed as symbiotics may as well be active main-sequence stars. We stress that low-resolution optical spectra may not always provide correct identification for these types of systems, and further high-resolution, multiwavelength, and timing observations may be required to understand the true nature of these sources.

M.Ö.A. acknowledges support from TÜBİTAK, The Scientific and Technological Research Council of Turkey, through the research project 109T736. J.A.T. acknowledges partial support from NASA through *Chandra* Award Number GO1-12046X issued by the *Chandra* X-ray Observatory Center, which is operated by the Smithsonian Astrophysical Observatory under NASA contract NAS8-03060. We thank the Turkish National Observatory of TÜBİTAK for running the optical facilities. We thank Dr. Timur Şahin for fruitful discussions. We also thank N. Masetti for his helpful comments on the source IRXS J174607.8-213333.

REFERENCES

Assafin, M., Andrei, A. H., Martins, R. V., et al. 2001, ApJ, 552, 380
Barbier, L., Barthelmy, S., Cummings, J., et al. 2005, GRB Coordinates Network, 4360, 1

Bird, A. J., Bazzano, A., Bassani, L., et al. 2010, ApJS, 186, 1B
Bodaghee, A., Rahoui, F., Tomsick, J. A., & Rodriguez, J. 2012, ApJ, 751, 113
Butler, S. C., Tomsick, J. A., Chaty, S., et al. 2009, ApJ, 698, 502
Cayrel, R., Faurobert-Scholl, M., Feautrier, N., Spielfieldel, A., & Thévenin, F. 1996, A&A, 312, 549
Chaty, S., Rahoui, F., Foellmi, C., et al. 2008, A&A, 484, 783
Cieslinski, D., Elizalde, F., & Steiner, J. E. 1994, A&AS, 106, 243
Corradi, R. L. M., Rodrguez-Flores, E. R., Mampaso, A., et al. 2008, A&A, 480, 409
Cutri, R. M., Skrutskie, M. F., van Dyk, S., et al. 2003, The IRSA 2MASS All-Sky Point Source Catalog, NASA/IPAC Infrared Science Archive http://irsa.ipac.caltech.edu/applications/Gator/
Deutsch, E. W. 1999, AJ, 118, 1882
Eaton, J. A. 1995, AJ, 109, 179
Friedjung, M., & Viotti, R. 1982, J. Br. Astron. Assoc., 93, 45
Gray, R. O., & Corbally, C. J. 2009, Stellar Spectral Classification (Princeton, NJ: Princeton Univ. Press)
Gunn, J. E., & Stryker, L. L. 1983, ApJS, 52, 121
Haisch, B. M., Schmitt, J. H. M. M., Rodono, M., & Gibson, D. M. 1990, A&A, 230, 419
Jacoby, G. H., Hunter, D. A., & Christian, C. 1984, ApJS, 56, 257
Jaschek, C., & Jaschek, M. 1995, The Behavior of Chemical Elements in Stars (Cambridge: Cambridge Univ. Press)
Kennea, J. A., Mukai, K., Sokoloski, J. L., et al. 2009, ApJ, 701, 1992
Kenyon, S. J. 1986, The Symbiotic Stars (Cambridge: Cambridge Univ. Press)
Kenyon, S. J. 1990, in ASP Conf. Proc. 9, Cool Stars, Stellar Systems, and the Sun: Sixth Cambridge Workshop, ed. G. Wallerstein (San Francisco, CA: ASP), 206
Kenyon, S. J., & Fernandez-Castro, T. 1987, AJ, 93, 938
Kenyon, S. J., & Webbink, R. F. 1984, ApJ, 279, 252
Kogure, T., & Leung, K.-C. 2007, The Astrophysics of Emission Line Stars (Berlin: Springer), 342
Krivonos, R., Tsygankov, S., Revnivtsev, M., et al. 2010, A&A, 523, 61
Lebrun, F., Leray, J. P., Lavocat, P., et al. 2003, A&A, 411, L141
Luna, G. J. M., & Sokoloski, J. L. 2007, ApJ, 671, 741
Luna, G. J. M., Sokoloski, J. L., Mukai, K., & Nunez, N. 2012, ATel, 3960
Masetti, N., Bassani, L., Bird, A. J., & Bazzano, A. 2005, ATel, 528
Masetti, N., Bassani, L., Dean, A. J., Ubertini, P., & Walter, R. 2006, ATel, 715
Masetti, N., Landi, R., Pretorius, M. L., et al. 2007, A&A, 331, 337
Masetti, N., Mason, E., Morelli, L., et al. 2008, A&A, 482, 113
Masetti, N., Parisi, P., Jimnez-Bailn, E., et al. 2012, A&A, 538, 123
Masetti, N., Parisi, P., Palazzi, E., et al. 2009, A&A, 495, 121
Mikołajewska, J., Acker, A., & Stenholm, B. 1997, A&A, 327, 191
Monet, D. G. 1998, BAAS, 30, 1427
Monet, D. G., Levine, S. E., Canzian, B., et al. 2003, AJ, 125, 984
Montes, D., & Martín, D. L. 1998, A&AS, 128, 485
Morgan, W. W., Kellman, E., & Hoffleit, E. 1943, Science, 97, 536
Motch, C., Warwick, R., Cropper, M. S., et al. 2010, A&A, 523, 92
Muerset, U., Wolff, B., & Jordan, S. 1997, A&A, 319, 201
Nespoli, E., Fabregat, J., & Mennickent, R. E. 2010, A&A, 516, 94
Oke, J. B. 1990, AJ, 99, 1621
Oke, J. B., & Gunn, J. E. 1983, ApJ, 266, 713
Osten, R. A., Drake, S., Tueller, J., et al. 2007, ApJ, 654, 1052
Paizis, A., Ebisawa, K., Takahashi, H., et al. 2009, PASJ, 61, 107
Paizis, A., Nowak, M. A., Chaty, S., et al. 2007, ApJ, 657, 109
Pereira, C. B., & Roig, F. 2009, AJ, 137, 118
Pettersen, B. R., & Hawley, S. L. 1989, A&A, 217, 187
Phillips, J. P. 2007, MNRAS, 376, 1120
Ratti, E., Bassa, C. G., Torres, M. A. P., et al. 2010, MNRAS, 408, 1866
Rodriguez, J., Tomsick, A. J., & Bodaghee, A. 2010, A&A, 517, 14
Rodriguez, J., Tomsick, A. J., & Chaty, S. 2008, A&A, 482, 731
Rodriguez, J., Tomsick, A. J., & Chaty, S. 2009, A&A, 494, 417
Roos, M. S., Boisson, C., & Joly, M. 1996, A&AS, 117, 93
Silva, D. R., & Cornell, M. E. 1992, ApJS, 81, 865
Skrutskie, M. F., Cutri, R. M., Stiening, R., et al. 2006, AJ, 131, 1163
Sugizaki, M., Mitsuda, K., Kaneda, H., et al. 2001, ApJS, 134, 77
Tomsick, J. A., Bodaghee, A., Chaty, S., et al. 2012, ApJ, 754, 145
Tomsick, J. A., Chaty, S., Rodriguez, J., Walter, R., & Kaaret, P. 2009, ApJ, 701, 811
Tomsick, J. A., Chaty, S., Rodriguez, J., et al. 2006, ApJ, 647, 1309
Walter, R., Lubiński, P., Paltani, S., et al. 2007, A&A, 461, 17
Winkler, C., Courvoisier, T. J.-L., Di Cocco, G., et al. 2003, A&A, 411, L1
Zhou, X. 1991, A&A, 248, 367